Preprint
UCRL-JC-148598

Electrochemical Behavior of Alloy 22 IN 5 M $CaCl_2$

G.O. Ilevbare

This article was submitted to
American Society of Mechanical Engineers Pressure Vessels and Piping Conference, Vancouver, Canada, August 4-8, 2002

May 30, 2002

U.S. Department of Energy

Lawrence
Livermore
National
Laboratory

DISCLAIMER

ELECTROCHEMICAL BEHAVIOR OF ALLOY 22 IN 5 M $CaCl_2$

G.O. Ilevbare
Yucca Mountain Project
Lawrence Livermore National Laboratory
7000 East Avenue
Livermore California 94550

ABSTRACT

The corrosion resistance of Alloy 22 (UNS No.: N06022) was studied in 5 M $CaCl_2$ electrolyte at various temperatures. Potentiodynamic polarization was used to examine the electrochemical behavior and measure the key potentials. Alloy 22 was found to be susceptible to localized corrosion in this high chloride [10M Cl^-] environment at temperatures as low as 60°C.

Keywords: Alloy 22, localized corrosion, pitting corrosion, crevice corrosion, temperature, electrochemical behavior, corrosion potential, cyclic polarization, chloride, Yucca Mountain, nuclear waste.

INTRODUCTION

This work is in support of the design and construction of the potential geological nuclear waste repository in Yucca Mountain Nevada. Therefore, the environmental considerations of importance are those pertaining to the design and construction of high-level radioactive waste packages for the Yucca Mountain Project (YMP). The design of the waste package as stipulated in the License Design Selection Report [1], calls for a double walled canister. The proposed material for the outer barrier of the waste package is Alloy 22 (Unified Numbering System (UNS) N06022), the corrosion resistant material (CRM). Alloy 22 is expected to provide a

reasonable level of "kinetic" immunity from general and localized corrosion for the waste packages under the prevailing environmental condition in Yucca Mountain. Kinetic immunity would ensure a low rate of passive dissolution, and negligible chance of generating damaging pits or crevices. The proposed material for the inner barrier of the waste package is stainless steel 316 (UNS S31603). The primary role of this layer is structural reinforcement [1].

The composition of the ground water (well water) found at Yucca Mountain is described in Table 1. It is referred to as J-13 [2-4]. The water is so named because it was drawn from a well designated J-13 in the Nevada test site, located near Yucca Mountain. The well draws from the same rock unit as Yucca Mountain. J-13 is benign to Alloy 22 for electrochemical testing especially over short periods of time [5, 6]. However, it is expected that under service conditions, the evaporative concentration of J-13 (from continuous wetting and drying cycles) due to the heat anticipated from the radioactive decay would result in a film of a more concentrated version of J-13 on the containers [4]. However, this process is expected to occur after a significant drop in temperature since the heat generated initially is expected to keep the repository in a fairly dry state for approximately 1000 years [7, 8].

Earlier studies of the localized corrosion behavior of Alloy 22 in concentrated simulated waters [9] shows that Alloy 22 in not susceptible to localized corrosion at temperatures up to 90°C. The susceptibility of alloy 22 is limited to transpassive dissolution of the oxide film. Extensive studies have been carried out on the effects of temperature (25 to 200 °C) and electrolyte composition (0.017 M chloride concentration ($[Cl^-]$) to saturation) on the critical breakdown potentials for localized corrosion on Nickel (Ni) alloys [10-22]. A decrease in temperature and $[Cl^-]$ increases the critical breakdown potential. An increase in concentration of alloying elements like tungsten (W), chromium (Cr) and molybdenum (Mo) also increases these breakdown potentials. The synergy between Cr and Mo in resisting localized corrosion is particularly effective in raising the breakdown potentials. Alloy 22 is more resistant to localized breakdown, and exhibits much lower corrosion rates compared with alloys such as 625 and 825 [12-14, 19, 24-27]. Consequently, more severe environments are required to initiate breakdown in Alloy 22 compared with Alloys 625 and 825.

In this study, electrochemical tests were performed to determine the effect of temperature on the electrochemical behavior of Alloy 22 in high a chloride containing electrolyte. Since Alloy 22 is very resistant to localized corrosion [12-14, 19, 24-27], very high chloride concentrations were essential in order to probe the bounds of susceptibility of this alloy. However, it should be noted that the ground water found in Yucca Mountain, contains a diverse mixture of oxyanions (Table 1). This will also be the case for any concentrated version of the ground water resulting from evaporative concentration [9]. Therefore, it is not expected that situations where only concentrated chloride solutions (which do not contain any other anions or oxyanions) will contact the surface of the containers will ever occur in Yucca Mountain. Apart from the fact that this array of species make the water chemistry and the possible specie/metal surface interactions complicated, some of the oxyanions present in the ground water of Yucca mountain (e.g., nitrate (NO_3^-), sulfate (SO_4^{2-}) have been implicated in inhibiting localized corrosion in stainless steels and nickel [28-38]. These oxyanions are present in appreciable concentrations (Table 1) compared with Cl^-, and would be expected to significantly affect the various critical potentials and the onset of localized corrosion on Alloy 22 under service conditions in Yucca Mountain. The preliminary results presented here highlight the results of corrosion potential (E_{corr}) measurements, as well as slow scan rate potentiodynamic polarization of Alloy 22 in 5 M $CaCl_2$ at various temperatures.

EXPERIMENTAL PROCEDURE

The material used in this study is Alloy 22. Its chemical composition as documented by the supplier appears in Table 2. The composition is consistent with the ASTM B-574 standard [39]. Two sample configurations were used in these experiments. Some of the samples were supplied in the form of 30.48 cm long rods with a diameter of 0.625 cm (Figure 1a). A 2.54 cm length of the sample was immersed in the electrolyte in the cell so that the total area of the sample immersed was ~5.38 cm^2. The samples were wet ground with 600-grit SiC paper (unless otherwise stated) and rinsed in distilled water before experimentation. These samples (rods) were used to study the susceptibility of Alloy 22 to pitting corrosion. The other sample configuration was supplied in the form of Multiple Crevice Assembly (MCA) specimens, which

look like lollipops (Figure 1b). The working surfaces of the MCA samples were used in the as-received state after degreasing with acetone and methanol. In the as received state, the working surfaces of the MCA samples were finished to a root mean square (RMS) roughness factor of between 2 and 4 with an air formed oxide film. The rest of the MCA consisted of Titanium (Ti) grade 2 nuts, bolts and washers, as well as ceramic crevice formers with multiple ridges (Figure 1c). The bolts were Teflon wrapped to prevent these hardware components from being in electrical contact with the specimen. Each crevice former had a total of 12 ridges on it, creating 12 different potential crevice sites on each face of the specimen, and a total of 24 potential sites in each assembly (Figure 1d). The assembly was tightened to a torque of 70 in-lb. Teflon tape inserts were placed between the ceramic crevice former and the MCA sample. This was done to fill in the micro voids created by the micro-rough surfaces of the sample and the ceramic crevice former, and to increase the possibility of producing a reproducibly tight crevice in all samples. The total surface area of the MCA specimen immersed in the electrolyte was 7.43 cm^2. This surface area included the area under the ridges of the crevice formers. The area under the 24 ridges of the crevice formers totaled 1.6 cm^2. In current density estimations, the surface area of 7.43 cm^2 was used. Therefore, the current density estimates for the MCA samples might be marginally lower than in reality. The MCA samples were used to study the susceptibility of Alloy 22 to crevice corrosion.

A three-electrode cell with a capacity of 1000 cm^3 was used for experimentation. The volume of electrolyte in the cell was about 900 cm^3. A saturated silver/silver chloride (SSC) (Ag/AgCl) electrode was the reference electrode. This electrode has a reference potential that is approximately 200 mV more negative than that of the standard hydrogen electrode (SHE). The reference electrode was maintained near room temperature by mounting it at the end of a Luggin probe, which had a water-cooled jacket around it. The water temperature in the cooling jacket was about 12°C. Thermal liquid junction calculations showed that potential variation caused by this phenomenon was in the order of mV (~10 mV maximum). Also, according to Macdonald et al., a high KCl concentration in the reference electrode tends to suppress thermal liquid junction potentials across the boundary between the high and low temperature solutions [40]. The liquid junction potential variations were therefore ignored in further analyses at this stage of the work

since they were thought to be negligible with regard to short term corrosion potential monitoring and potentiodynamic polarization tests. The counter electrode was made of platinum (Pt) foil. Electrical connection was achieved through a piece of Pt wire spot welded to the foil. The temperature of the electrolyte was maintained by immersing the glass cell in a heating bath filled with silicon oil so that the level of the electrolyte in the cell was the same as, or below the level of the silicon oil surrounding the cell. The sample was immersed in the cell after the electrolyte had attained the desired temperature. The temperature was taken before and after the experiment with a thermocouple immersed into the electrolyte. Electrochemical measurements were carried out using a potentiostat. The measurements included the recording of the corrosion potential (E_{corr}), for 24 hours (unless otherwise stated), followed by cyclic potentiodynamic polarization immediately afterwards. Cyclic polarization was started approximately 100 mV below E_{corr}, and continued until the current density from the sample reached a maximum of up to 30 $mAcm^{-2}$, or a maximum of 1.3V (SSC) before the scan was reversed. The sweep rate in the forward and backward directions was 0.1667 mVs^{-1} (600 mV per hour). Deaerated 5 M $CaCl_2$ was the electrolyte used in these experiments. The pH of this electrolyte was about 6. Nitrogen gas (N_2) was pumped through the electrolyte for at least one hour before and throughout the experiments at a rate of 100 cc/minute. All electrolytes were prepared using certified American Chemical Society (ACS) grade chemicals.

RESULTS

The Corrosion Potential (E_{corr})

Figure 2 shows some examples of 24-hour E_{corr} transients of Alloy 22 in 5 M $CaCl_2$ at 60, 75 and 90 °C. The values of the E_{corr} do not significantly differ from each other as the temperature of the electrolyte increased from 60 to 90 °C in both sample configurations (rods and MCA). Amongst the transients shown in Figure 2, the difference between the highest and the lowest E_{corr} after a 24-hour immersion period was about 60 mV. The evolution of the E_{corr} did not follow a particular pattern over this 24-hour period. On some samples the E_{corr} stayed fairly constant. On a number of samples it increased with time, while on some others it decreased with time. This pattern was observed irrespective of the temperature.

Figure 3 shows the E_{corr} values of all the experiments carried out plotted as cumulative probability distributions. The values plotted were recorded at the 24-hour mark of the experiments (i.e., at the 86 400 s mark). The distribution of the E_{corr} on the rod samples at 90°C has a long tail. This long tail is accounted for by only 2 of the 5 values, which make up the distribution. The highest E_{corr} value in Figure 3 was registered at 60°C on a rod sample, followed by at 75°C and then at 90°C also on rod samples. There was more scatter in the values of the E_{corr} of the rod compared with the MCA samples. While the rod samples tend to show that the E_{corr} in 5 M $CaCl_2$ decreased with temperature, no such distinction or separation was observed in the MCA samples. The reason(s) for this observation are not clear at this time. Nonetheless, the distributions of the E_{corr} values in the systems under study were very close. There is a difference of only about 60 mV at the 50-percentile mark between the highest and lowest E_{corr} values (Figure 3).

Potentiodynamic Polarization

Figures 4 and 5 show representative polarization curves for Alloy 22 at 60 and 90°C in deaerated 5 M $CaCl_2$ for rod and MCA samples respectively. No curves were shown for 75°C because they are largely similar to those taken at 90°C. The horizontal line across the figures lies at the current density of 2×10^{-5} Acm^{-2} (20 μAcm^{-2}). This was the threshold current density at which the critical breakdown potential[a] was taken. At a current density of 20 μAcm^{-2}, stable pitting or crevice corrosion would usually have commenced as evident from work carried out by various authors where pitting or crevice breakdown potentials were measured for various stainless steels, nickel and Alloy 22 [12,13,42,43]. This threshold value of 2×10^{-5} Acm^{-2} is arbitrary, and was used only as a reference point as a basis for comparison of the data in this paper. It bears no other significance.

The permanent increases in current density from the passive region (or from passive current density level) observed in the polarization curves in Figures 4 and 5 show that alloy 22 is

[a] "Critical breakdown potential", E_{crit}, as employed here is used to denote the potential(s) at which any type of breakdown of the passive film whether localized (e.g., pitting or crevice corrosion), or due to general dissolution, or transpassive dissolution of chromium or molybdenum occurs.

susceptible to localized corrosion in deaerated 5 M $CaCl_2$ at 60 and 90 °C. An inspection of the samples under an optical microscope confirmed the presence of localized corrosion damage on the samples. On the rod samples (Figure 4), the attack was either consistent with pitting, or what looked like localized etching as (Figure 6a). The physical damage to the sample at 90 °C (Figure 6a) was the severest, while damage at 60 °C was the least severe of the three temperatures tested. At 75 and 90 °C, once the attack, which was indicated, by a permanent rise in current from passive state started, it continued until the potential scan was reversed (Figure 4). At 60°C, some of the samples experienced a drop in current density after an initial rise in current density. This drop in current density fell to or below initial passive current density levels, and created an "anodic peak" or "hump" as observed in Figure 4. Figure 4 also shows an example of when there was no drop in current density during the forward scan on Alloy 22 at 60°C after the first rise in current density. In cases where there was a fall in the current density back to or below original passive current density levels after an initial current increase, it appears that the localized breakdown of the samples (either by etch-like attack or pitting) took place before or at the current density maximum of the initial anodic peak as the current density rose. This conclusion was arrived at through the observation of the surface of samples, which broke down in the potential region corresponding to the region of current rise in the anodic peak. The current densities that were reached before the drop in current density were sometimes as high as 30 $mAcm^{-2}$ (Figure 5). The fall in the passive current density to near the original passive current density (below 2×10^{-5} Acm^{-2}) showed that a reasonably good passive film had been formed upon the drop in current density. On further increase of the potential, the sample then eventually experiences another increase in current density this time due to transpassive dissolution. Figure 6b show an example of what the surface of one such sample looked like after the initial current decrease (after the hump), and then transpassive dissolution. In this case, the mode of localized break down was consistent with pitting corrosion. The dark uniform coloration on the rod corresponding to the area immersed in the electrolyte is corrosion product from transpassive dissolution. This behavior did not occur at 75 or at 90 °C. The primary mode of localized attack at 90°C was localized etch-like attack, while at 60°C; it tended to be either of the two modes (etch-like attack and pitting corrosion).

A similar behavior was observed on the MCA samples (Figure 5). In these samples, (which were used to study the susceptibility of Alloy 22 to crevice corrosion) it was also observed that the samples tended to experience a fall in current density after the initial increase in current density. No fall in current density took place in the forward sweep at the higher temperatures of 75 and 90 °C. As with the rod samples, there was a fall in current density back to near passive current density levels (below 2 x 10^{-5} Acm^{-2}) with the MCA samples. The severity of the attacks in terms of the physical damage observed when the MCA was taken apart increased with increase in temperature. Apart from the mode of localized attack between the rod and MCA samples, the other observable difference was in the value of the passive current density. The passive current density of the MCA samples was higher than the threshold current density used for the determination of the breakdown potential at all the temperatures tested.

Figures 7 and 8 are cumulative probability plots of the critical breakdown potential E_{crit}, and the E_{corr} of the rod and MCA samples respectively as a function of potential at 60, 75 and 90°C. In these graphs, two different criteria were used to determine the critical breakdown potential. One of the methods was the threshold current density method in which the potential, which coincided with the threshold current density of 2 x 10^{-5} Acm^{-2}, was taken as the critical breakdown potential. As seen from Figures 4 and 5, this method did not take into account the fall in current density in the "hump" of the samples polarized at 60°C on both the rod and MCA samples, and neither did it take into consideration the fact that the current density in the passive region on the MCA samples at all the temperatures tested were generally above the threshold current density. To address this issue, another method was used to measure E_{crit}. In this second method, E_{crit} was taken as the potential that coincided with the onset of the first permanent rise in current density from the passive state. An asterisk (*) is used to denote the E_{crit} values obtained by the second method. In rod samples (Figure 7), only the data derived from the 60°C measurements by the second method are plotted. The differences observed between the E_{crit} values measured by the first and second methods at 75 and 90°C were not as significant as those observed at 60°C. In the MCA samples (Figure 8), data from both measurement methods are presented at all temperatures.

The E_{crit} due to pitting and etch-like breakdown (from rod samples in Figure 7) were much higher than those due to crevice attack obtained from the MCA samples (Figure 8). E_{crit} increased as temperature decreased in both sample configurations. The difference between the highest E_{corr} and the lowest E_{crit} obtained on the rod samples was about 300 mV (Figure 7). With the MCA samples, the difference between highest E_{corr} and the lowest E_{crit} when a current density threshold criterion was used was about 25 mV, and about 200 mV if the first permanent rise in current density from the passive state (second method) was used to obtain the E_{crit}. It should be noted that at 60 °C the E_{crit} values due to localized breakdown were not separated from those due to transpassive dissolution.

DISCUSSION

Twenty four-hour measurements of the E_{corr}, and slow scan potentiodynamic polarization experiments are inadequate to predict the behavior of Alloy 22 under repository conditions for geologically long periods of time (in the case of Yucca Mountain, 10,000 years). However they offer an insight as to how Alloy 22 will behave under service condition. These relatively short laboratory experiments are also essential for modeling exercises, which are an important component of predicting the long-term viability of this alloy for the purpose of high-level nuclear waste containment.

From the data in Table 1 (composition of J-13 well water), it is highly unlikely that under the environmental conditions in Yucca Mountain, the containers will ever be in contact with solutions of an "only" chloride composition. For this reason, 5 M $CaCl_2$ (10 M Cl^-) must be regarded as a theoretical worst-case scenario environment with little possibility of its presence (without the presence of any other anions or oxyanions) under real life repository conditions. Earlier work showed that Alloy 22 is not susceptible to localized corrosion in simulated concentrated (J-13) environments [9].

From the data presented, it is not possible to say with certainty what trend the evolution of the E_{corr} of Alloy 22 will follow over longer exposure periods of time, i.e., whether it will rise,

fall, or remain fairly constant with time, as all these trends were exhibited by both sample configurations tested at all temperatures (Figure 2). Nonetheless, it is quite clear that there is a distinction between the E_{corr} and the breakdown potential of Alloy 22 (Figures 4, 5, 7 and 8) in 5 M $CaCl_2$ at temperatures of up to 90°C. It is vital that the E_{corr} of the Alloy 22 stays within the passive region over long periods of time to guarantee kinetic immunity. A vital question that remains unanswered is whether the E_{corr} will ever rise enough to reach and exceed the critical breakdown potential. Longer term (several years) E_{corr} monitoring experiments will be required to answer this question.

It is not surprising that the critical breakdown potential of Alloy 22 in 5 M $CaCl_2$ decreased as temperature increased (Figures 4, 5, 7 and 8). What is surprising is the ability of Alloy 22 to recover from the high current density excursions (which suggest localized breakdown) at 60 °C (Figures 4 and 5). This is a demonstration to the excellent corrosion resistance of Alloy 22. The reason(s) why the pits and crevices (Figures 7 and 8) generated at this temperature experience difficulty in reactivating before the onset of transpassive dissolution is not fully understood at this time. This will be one of the subjects of future work. The etch-like localized attack observed on the rod samples at all temperatures, but most severe at 90°C can only be attributed to the highly aggressive conditions of the environment.

The reason(s) why the passive current density of the MCA samples was higher than the threshold current density used for the determination of the breakdown potential at all the temperatures tested is not clear at the moment. However, one possibility is that there is a more active zone on the edge (non working surface of the sample), which has a slightly different oxide film composition (physical and/or chemical) from that of the working surface.

The higher critical breakdown potential exhibited by the rod samples compared with the MCA samples shows that it is more difficult to initiate and propagate a localized corrosion event on an open surface of Alloy 22 compared with an occluded surface. This confirms that in terms of localized corrosion, crevice corrosion is much more of a threat (more easily initiated) to Alloy 22 than pitting corrosion. At the 50-percentile probability mark (Figure 7 and 8), the rods had a critical breakdown potential of about 170, 105 and 20 mV at 60, 75 and 90 °C respectively, while

the MCA samples had a critical potential of about -280 mV at all the three temperatures if the threshold current density (2×10^{-5} Acm^{-2}) method was used to asses E_{crit}. It is observed that at 60 °C, when the second method was used to determine the E_{crit} of the rod samples is lower than that of the MCA samples (at 50-percentile probability mark breakdown occurs at, ~500 and ~700 mV respectively). A possible reason for why the onset of transpassive passive dissolution is sooner on the rod compared to the MCA samples is probably because the presence of the ceramic former acted as a barrier to diffusion.

CONCLUSIONS

- Alloy 22 is susceptible to localized corrosion in 5 M CaCl2 at temperatures as low as 60 °C.
- The onset of localized corrosion is shifted to higher potentials as temperature decreased.
- Alloy 22 exhibited an anodic peak or "hump" at between 200 and 300 mV at 60°C. This was not observed at 75 and 90 °C.
- Localized corrosion initiated more readily on Alloy 22 in and around occluded areas compared with open surface in 5 M $CaCl_2$ at temperatures up to 90 °C.

REFERENCES

1. Civilian Radioactive Waste Management (CRWMS) Management and Operating Contractor (M&O), Licensing Application Design Selection (LADS) Report, B00000000-01717-4606-00123 Rev. 01 ICN 01, CRWMS M&O, Las Vegas, 1999.
2. J. Harrar, J. Carley, W. Isherwood and E. Rabeer, in Report of the Committee to Review The Use of J-13 Well-water in the Nevada Nuclear Waste Storage Investigations, UCID-21876, Lawrence Livermore National Laboratory, January 1990.
3. F. Wang, G.E. Gdowski, J. Estill, S. Gordon, S. Doughty, K. King and D. McCright, Corrosion'98, 1998 Paper No. 161.

4. N.D. Rosenberg, G.E. Gdowski, and K. G. Knauss, Applied Geochemistry, 2001. **16**: p.1231.
5. K.A. Gruss, G.A. Cragnolio, D.S. Dunn and N.Sridhar, Corrosion '98, 1998, Paper No. 149.
6. S.J. Lukezich, The Corrosion Behavior of Ni-Base High Performance Alloys in Simulated Repository Environments, MS Thesis, The Ohio State University 1989.
7. M. H. Wilde, and D.E. Wilde, Corrosion Science, 1993. **34**: p. 433.
8. D.W. Shoesmith, B.M. Ikeda, F. King, and S. Sunder, in, Prediction of Long Term Behavior for Radioactive Nuclear Waste Disposal, Proceedings of the CORROSION/96 Research Topical Symposia," Sponsored by the NACE Research Committee, 1996, p.101.
9. G.O. Ilevbare T. Lian and J.C. Farmer, Corrosion 2002, Paper No. 02539.
10. J. Postlethwaite, R.J. Scoular , and M.H. Dobbin,. Corrosion, 1988. **44**(4): p. 199.
11. G.A. Cragnolino and N. Sridhar. Corrosion, 1991. **47**(6): p. 465.
12. B. A. Kehler, G.O. Ilevbare and J.R. Scully Corrosion 2000, Paper No. 00182
13. B. A. Kehler, G.O. Ilevbare and J.R. Scully Corrosion 2001, Paper No. 01141
14. B. A. Kehler, G.O. Ilevbare and J.R. Scully Corrosion 2001, Crevice Corrosion Behavior, of Ni-Cr-Mo Alloys: Comparison of Alloys 625 and 22, NACE Topical Research Symposium, March 2001, p.30.
15. S.J. Mulford and D. Tromans, *Crevice Corrosion of Nickel-Based Alloys in Neutral Chloride and Thiosulfate Solutions.* Corrosion, 1988. **44**(12): p. 891.
16. R.S. Lillard, M.P. Jurinski, and J.R. Scully, *Crevice Corrosion of Alloy 625 in Chlorinated ASTM Artificial Ocean Water.* Corrosion, 1994. **50**(4): p. 251.
17. E.L. Hibner, Corrosion'86, 1986, Paper No. 181.
18. E. L. Hibner, Materials Performance, 1987. **26**(3): p. 37.
19. K.A. Gruss, G.A. Cragnolino, D.S. Dunn and N. Shridhar, *Repassivation Potential for Localized Corrosion of Alloys 625 and C22 in Simulated Repository Environments*, 1998, U.S. Nuclear Regulatory Commission (Washington, D.C.) and Center for Nuclear Waste Regulatory Analyses, Southwest Research Institute (San Antonio, TX),
20. D.S. Dunn, G.A. Cragnolino, and N. Sridhar, Corrosion, 2000. **56**(1): p. 90

21. N. Sridhar and G.A. Cragnolino, *Applicability of Repassivation Potential for Long-Term Prediction of Localized Corrosion of Alloy 825 and Type 316L Stainless Steel.* Corrosion, 1993. **49**(11): p. 885.
22. G.A. Cragnolino, *Assessment of Localized Corrosion of Alloys 825, 625, and C-22 for HLW Containers*, 1998, Waste Package Degradation Expert Elicitation Workshop
23. H.P. Hack, Materials Perfomance, 1983. **22**, (6): p.24.
24. G.E. Gdowski Survey of Degradation Modes of Four Ni-Cr-Mo Alloys UCRL-ID-108330, 1991. p.30-31.
25. Haynes International, Inc., Product Brochure H-200B, Haynes international Inc. Kokomo, IN, 1987. p.15.
26. Haynes International, Inc., Product Brochure H-2019C, Haynes international Inc. Kokomo, IN, 1988. p.22.
27. J. C. Farmer, D. McCright, G.E. Gdowski, F. Fang, T. Summers, P. Bedrossian, J. Horn, T. Lian, J. Estill, A. Lingenfelter, and W. Halsey, General and Localized Corrosion of Outer Barrier of High-Level Waste Container in Yucca Mountain, May 2000. Preprint UCRL-JC-138890, Lawrence Livermore National Laboratory, Technical Information Department Digital Library.
28. H.H Uhlig and J.R. Gilman, Corrosion, 1964. **20**: p.289t.
29. H. P. Leckie and H.H. Uhlig, J. Electrochem. Soc., 1966. **117**: p. 1152.
30. I.L. Rozenfeld, and I.S Danilov, Corrosion Science, 1967. **7**: p.129.
31. E.A. Lizlovs and A.P. Bond, J. Electrochem Soc., 1969. **116**: p.574.
32. Z. Szklarska-Smialowska, Corrosion Science, 1971. **11**: p.209.
33. Z. Ahmed, Corrosion, 1977. **33**: p.161.
34. H.H. Strehblow, and B. Titze, Corrosion Science, 1977. **17**: p.461.
35. H.C. Man and D. R. Gabe, Corrosion Science, 1981. **21**: p.713.
36. R.C. Newman and T Shahrabi, Corrosion Science, 1987. **27**: p.827.
37. H. Yashiro and K. Tanno, Corrosion Science, 1990. **31**: p. 485.
38. P.C. Pistorius, and G.T Burstein, Corrosion Science, 1992. **33**: p.1885.
39. ASTM B574, Annual Book of ASTM Standards, Nonferrous Metal Products, 2000. Volume 02.04, p.531,. American Society of Testing and Materials, West Conshohocken, PA.

40. D.D. MacDonald, A.C Scott, and P. Wentrcek, J. Electrochem. Soc., 1978. **126**: p.908.

41. M. Pourbaix, in Atlas of Electrochemical Equilibria in Aqueous Solutions, 1974. p.97. National Association of Corrosion Engineers, Houston TX.).

42. M, Karaminezhaad-Ranjbar, J. Mankowski, and D.D. MacDonald, Corrosion, 1985. **41**: p.197.

43. H. Guyader, V. Debout, and A.M. Grolleau, Crevice Corrosion of Ni base alloys and Highly Alloyed Stainless Steels in Sea Water in EUROCORR '99 Proceedings [EUROCORR '99 Proceedings], Sept. 1999. Event No. 227, p. 200. DECHEMA, Chemische Technik und Biotechnologie e.V., Frankfurt am Main, Germany.

ACKNOWLEDGEMENTS

The Department of Energy Office of Civilian Radioactive Waste Management (OCRWM) sponsored this work. This work was done under the auspices of the U.S. Department of Energy (DOE) by the University of California, Lawrence Livermore National Laboratory (LLNL) under contract No. W-7405-Eng-48. This work is supported by Yucca Mountain Site Characterization Project, LLNL. Technical comments by Daniel McCright and Raul B. Rebak.

Table 1. Chemical composition (in mg/l) of J-13 well water.

Ion	J-13 pH 7.4
K^+	5.04
Na^+	45.8
Mg^{2+}	2.01
Ca^{2+}	13.0
F^-	2.18
Cl^-	7.14
NO_3^-	8.78
SO_4^{2-}	18.4
HCO_3^-	128.9
SiO_3^{2-}/Si	61

Table 2. Chemical composition of Alloy 22 (UNS No. N06022) given in weight percent.

Element	Actual Composition	ASTM Requirements (ASTM B576)	
		Minimum	Maximum
Mo	13.1	12.5	14.5
Cr	22.3	20.0	22.5
Fe	3.4	2.0	6.0
W	2.9	2.5	3.5
Co	0.8	0.0	2.5
C	0.004	0.000	0.015
Si	0.06	0.00	0.08
Mn	0.29	0.00	050
V	0.15	0.00	0.35
P	0.01	0.00	0.02
S	<0.01	0.00	0.02
Ni	Balance	Balance	Balance

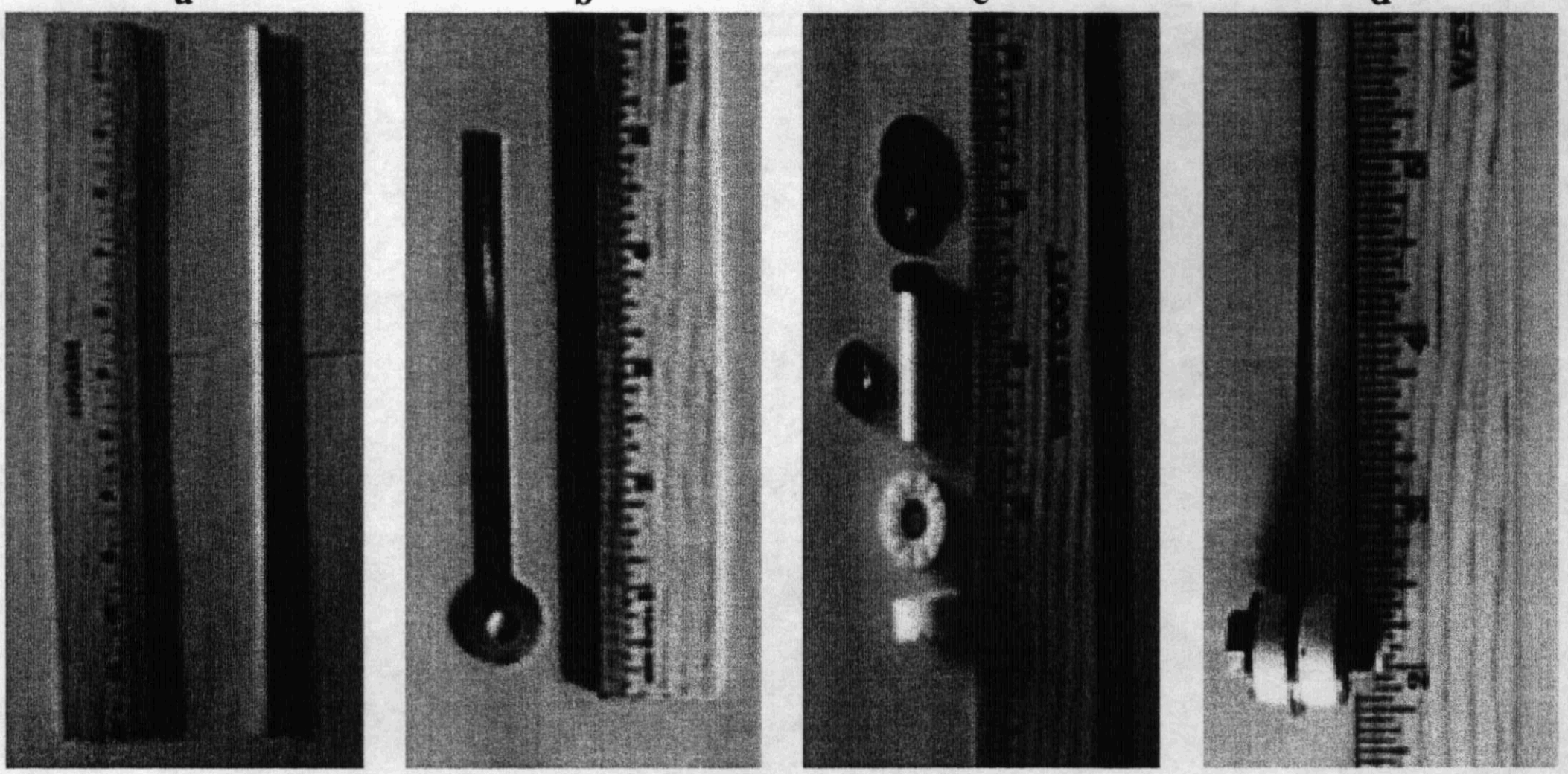

Figure 1. **a**) Rod sample. **b**) Multiple crevice assembly (MCA) sample (lollipop). **c**) Ti (grade 2) bolt, nut and washer used for the MCA. Bolt is wrapped with Teflon tape for electrical insulation. **d**) Fully assembled MCA sample.

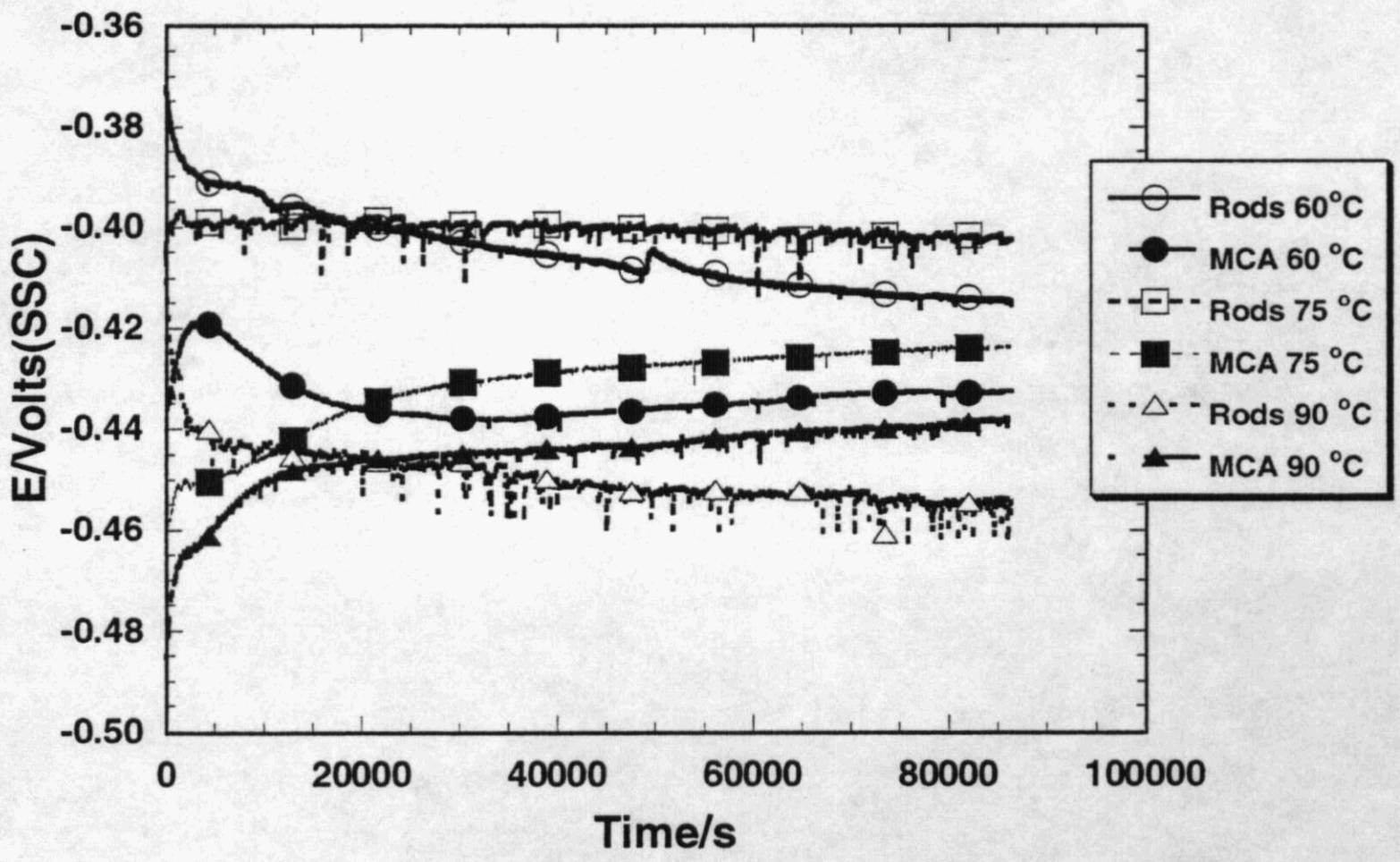

Figure 2. E_{corr} transients of Alloy 22 (rods and MCA) in deaerated 5 M $CaCl_2$ at 60, 75 and 90°C over a 24 hours period.

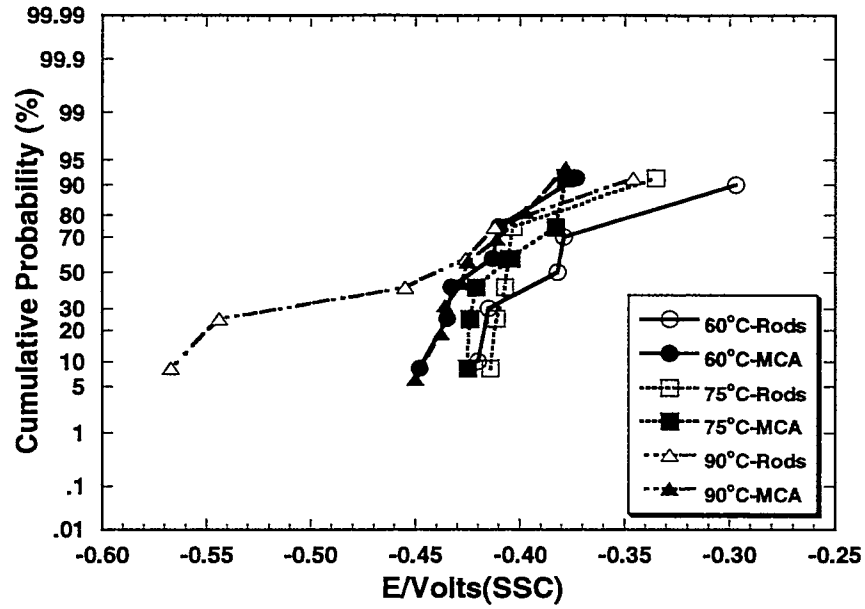

Figure 3. E_{corr} of Alloy 22 in 5 M $CaCl_2$ from rods and MCA samples presented as a probability plot.

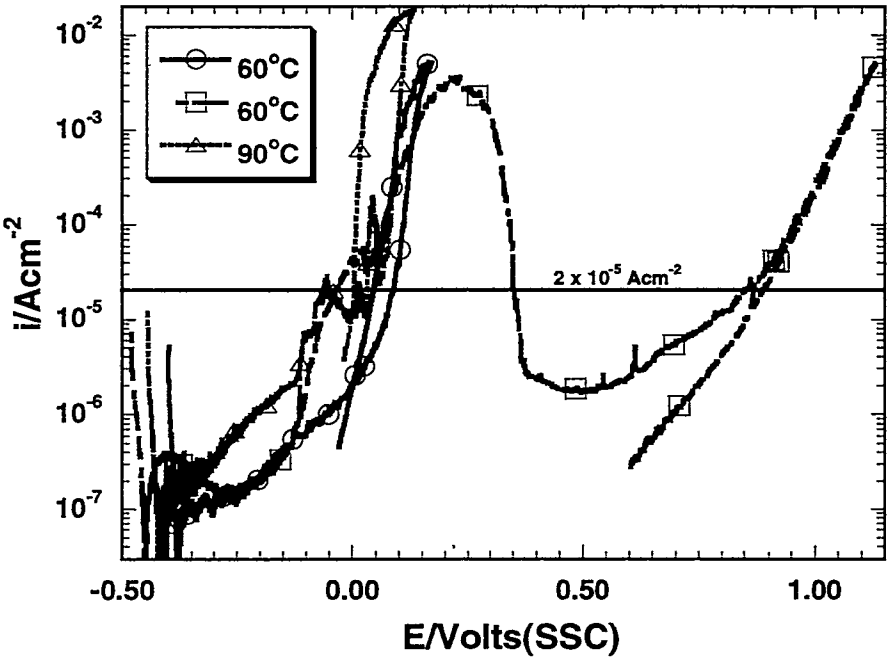

Figure 4. Polarization curves of Alloy 22 (rod samples) in 5 M $CaCl_2$ at 60 and 90°C. Sweep rate: 0.1667 mV/s. Samples were finished with 600 grit SiC paper.

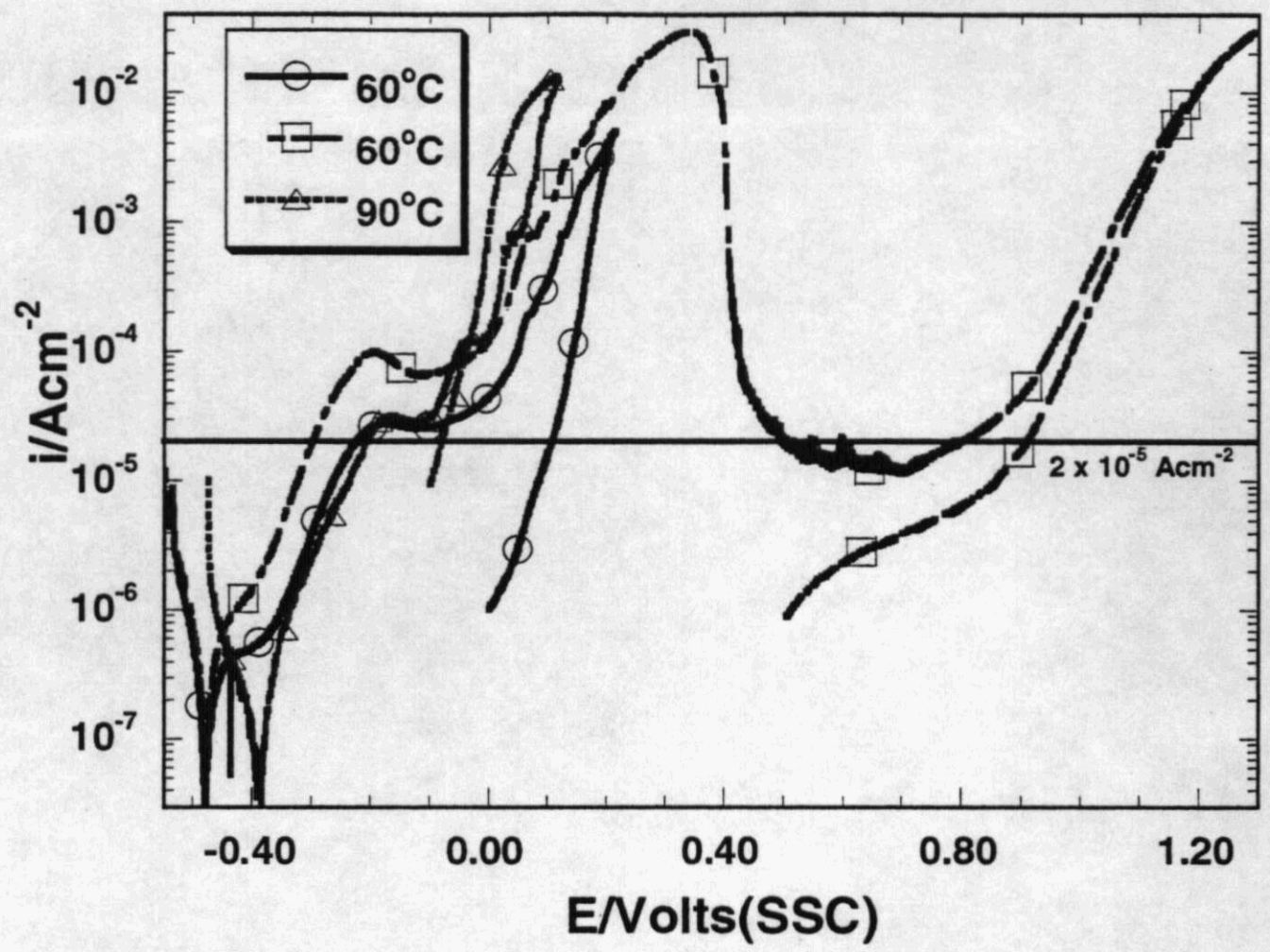

Figure 5. Polarization curves of Alloy 22 (MCA samples) in 5 M $CaCl_2$ at 60 and 90°C. Sweep rate: 0.1667 mV/s. The working surfaces of samples were used in the as received condition.

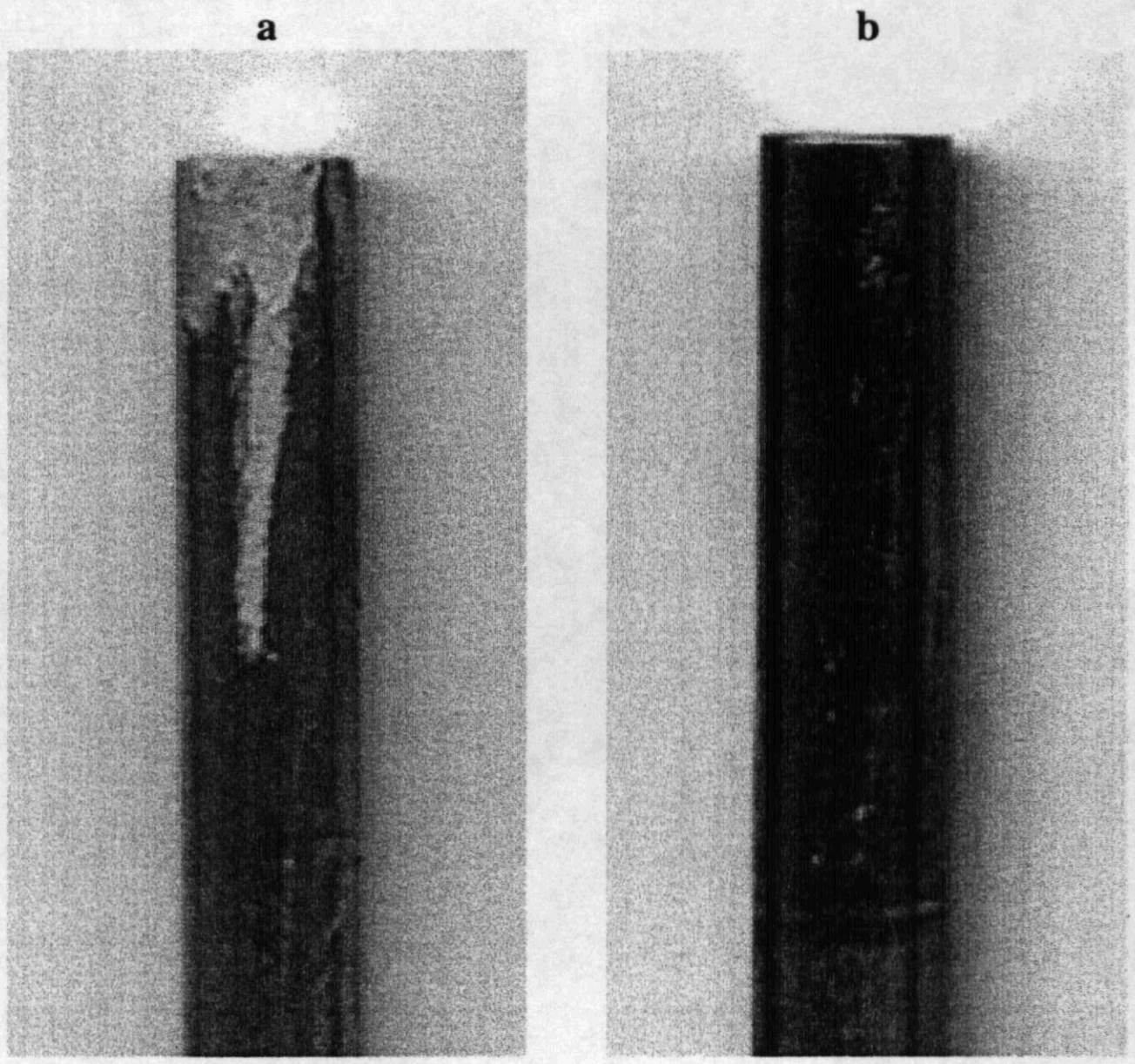

Figure 6. Alloy 22 rod samples after polarization in 5 M $CaCl_2$ at **a**) 90 °C, and **b**) 60°C. At 90°C (a) the etch-like attack is very prominent. This sample did not experience a drop in current density on the forward scan. At 60°C (b), this sample underwent pitting corrosion, followed by a drop in current density of the pits, and then transpassive dissolution, as evident by the uniform dark coloration of the rod due to transpassive dissolution products.

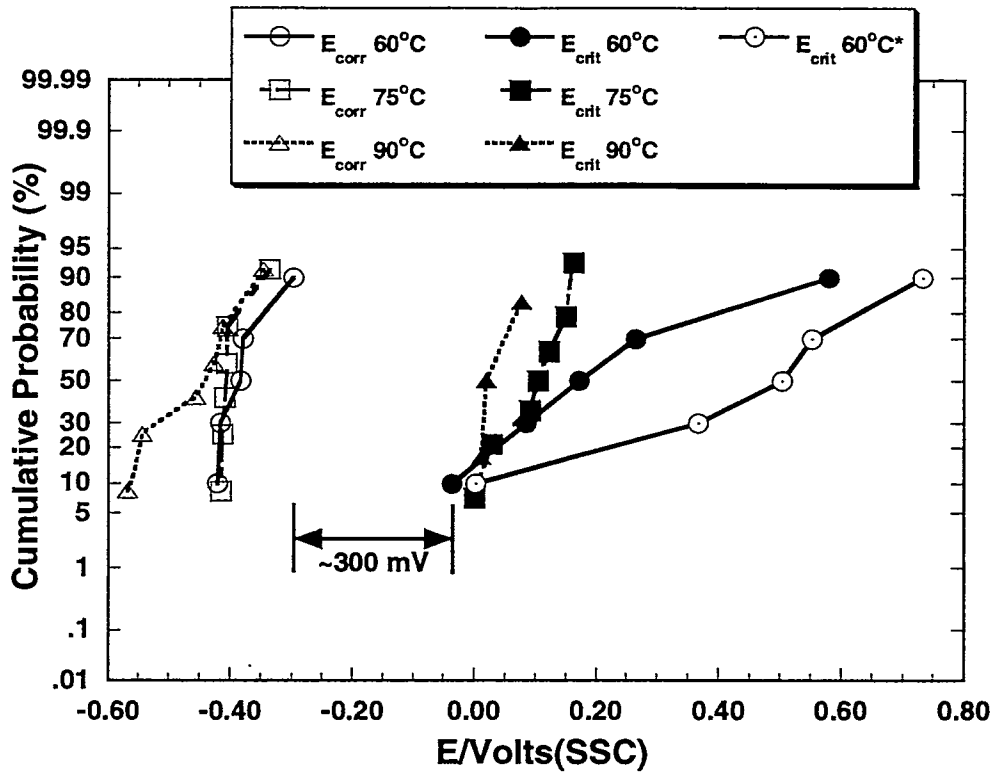

Figure 7. E_{corr} and critical breakdown potential, E_{crit}, of Alloy 22 in 5 M $CaCl_2$ from rod samples presented as a cumulative probability plot.

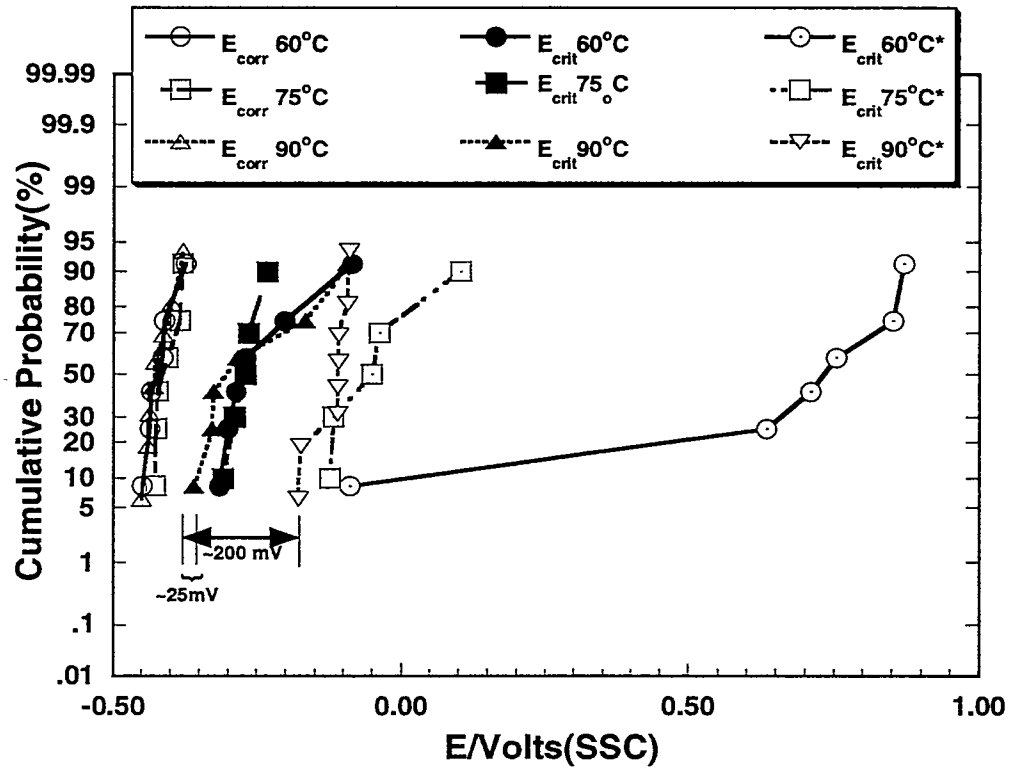

Figure 8. E_{corr} and critical breakdown potential, E_{crit}, of Alloy 22 in 5 M $CaCl_2$ from MCA samples presented as a cumulative probability plot.